DOI: 10.13009/EUCASS2017-603

Development of New Analytical Models of Pressure and Heat Transfer Distributions on Space Debris Uncontrolled Atmospheric Entry: Planar Bodies

Y.Prévereaud, J-L.Vérant*, J.Annaloro**, S.Galera****
**ONERA – The French Aerospace Laboratory*
2 avenue Edouard Belin – 31055 Toulouse – France
***CNES – The French Space Agency*
18 avenue Edouard Belin – 31401 Toulouse – France
****ALTRAN SO*
4 avenue Didier Daurat – 31700 Blagnac – France

Abstract
Few studies have yet considered the wall pressure and heat flux distribution over a flat plate assuming perfect gas to non-equilibrium flow conditions gas regarding the flight point, the attitude (angle of attack, side slip angle) and the size of the planar surfaces. One of them performed during 1950's by Hankey *et al.* [27] suggested a very interesting analytical approach based on Eckert reference enthalpy to describe heat flux distribution over a flat plate. However, this formulation can only be applied under limited conditions. In this context, formulations proposed in open literature or internally at CNES and ONERA in Spacecraft-Oriented Codes for debris re-entry scenarios, such as PAMPERO and FAST/MUSIC respectively, have highlighted the disparity or the weak performance of Newtonian-like pressure and heat flux correlations computed so far. Therefore, new analytical models have been developed and successfully compared to CFD simulations as a better update to former models. These models based on a wide in-house CFD database (ONERA CEDRE Navier-Stokes multi-physics Platform) have been tested for various flow conditions according to the debris flight points trajectory including different gas flow assumptions for the shock layer physics (perfect gas, thermochemical equilibrium and non-equilibrium real gas), the attitude and the size (length, width, height) of the planar surfaces under the scope and of interest for debris flight physics.

1. Introduction

Since 1957 and the orbital performance of the soviet satellite Spoutnik-1, the human activity in space has generated a great number of space debris. A large part of the orbital debris ranging from ten microns to several meters executes an atmospheric entry due to atmospheric drag in LEO and lunisolar perturbations in HEO (acting generally with atmospheric drag). Indeed, amongst the 27 044 catalogued objects between 1957 and 2006, 18 051 entered into the atmosphere, leaving around 8993 catalogued objects spread out in orbit [1]. Between 1957 and 2017 about 75% of all the larger objects ever launched have re-entered [2]. Only a small percentage was subjected to an intentional deorbiting or reached the ground under control. Currently, only few of very large objects cross Earth's atmosphere per year. Objects of moderate size, 1 m or above, re-enter around once a week, while an average of two small tracked debris objects re-enters per day. Between 10 and 40 % of the debris mass are estimated to have reached Earth surface [3], representing a potential threat to ground safety. An estimate of the total causality area becomes a major issue for all space actors and especially for CNES which is in charge of ensuring the right application of the French Space Operation Law (LOS) that will enter into force by 2021 for French satellites and launchers operators as well as launching operations from French Guyana spaceport.
These space actors have developed tools dedicated to the prediction of the ground risk generated by space debris atmospheric re-entry. However, high fidelity physical models as those of CFD tool (Fluid mechanics equations) cannot be applied to characterize a whole trajectory described by hundreds of points amongst thousands into a Monte Carlo procedure. Only a strategy based on relevant and reliable reduced models is acceptable for debris risk analysis in terms of computing time and computing capability. These engineering tools can be separated into two categories: Object-Oriented Codes and Spacecraft-Oriented Codes. Object-Oriented Codes consider individual satellite parts

DOI: 10.13009/EUCASS2017-603

only. In other words, this kind of code assumes that at a given altitude the satellite is decomposed into its elementary units. Object-Oriented Codes reduce the complex analysis of the atmospheric re-entry of a spacecraft to the simple analysis of its most critical parts, which must be previously defined by the user. This approach considerably simplifies the preliminary work. The fragmentation altitude discussed in [14] is usually fixed between 75 and 85 km. The described Object-Oriented Codes into open literature are DAS (NASA) [4], ORSAT (NASA) [4], ORSAT-J (JAXA) [5], DRAMA/SESAM (ESA) [6], DEBRISK (CNES) [7], DRAPS (China) [8], ASTOS/DARS (ESA) [9], and SAPAR (SouthKorea) [10].
On the other side, Spacecraft-Oriented Codes model the whole satellite into the most realistic design. The fragmentation model generates the fragments under the harsh environment encountered during the re-entry. After each break-up process, each fragment is analysed individually by completing oxidation/ablation understanding and modelling. SCARAB (HTG) [11], PAMPERO (CNES) [12] and FAST/MUSIC (ONERA) [13] are some of the known European Spacecraft-Oriented Codes.

A Mutual Interest Project (PIC) between ONERA and CNES has been entered into action to provide representative analytical models of the aerothermodynamic phenomena occurring during atmospheric re-entry of a class of simple but most of representative geometries of space debris as thick flatted-plates, boxes, burnthrough spheres and cones, cylinders,…etc. The present paper proposes a survey of the first step of the project that focuses on the modeling of the wall pressure and heat flux distribution on planar surfaces representative of space debris, such as solar panels, pressure monitoring modules, which can be represented by thick flatted plates or boxes.

3. Analysis of the numerical simulations

3.1. Presentation of the numerical simulations

ONERA developed an important database composed of around seventy 2D and 3D Navier-Stokes numerical simulations obtained with its multiphysics code CEDRE. Firstly, this numerical database aims at analyzing the physical phenomena occurring around thick flat plates or boxes in hypersonic flow regime. In particular, the influence of the flight points, the angle of attack (0°, 5°, 10°, 15°, 20°, 25°, 30°, 45°, 90°), the sizes of the flat plate (length, width, height) and the curvature radius of its edges on the wall pressure and heat flux distribution are studied. Secondly, the numerical results have been compared to the analytical models in use in PAMPERO, FAST/MUSIC and open literature (see §4). The objective is then to identify the limits of the current models and develop new ones more representative (see §5).

3.1.1. Mesh description

2D and 3D meshes, realized with ICEM, consist of around 100 000 elements and 8 millions of elements respectively. A cut slice of the mesh can be viewed in Figure 1. The mesh follows the shape and the position of the shock for a better capture of the strong shock (blue zone in Figure 1). The mesh is adapted in accordance with modified upstream flow (velocity, altitude, angle of attack) along re-entry path. A boundary layer has been built at the wall to properly capture gradients. The first layer consists of 1 μm elements, others are increased by a factor of 1.25 within a geometrical suite.

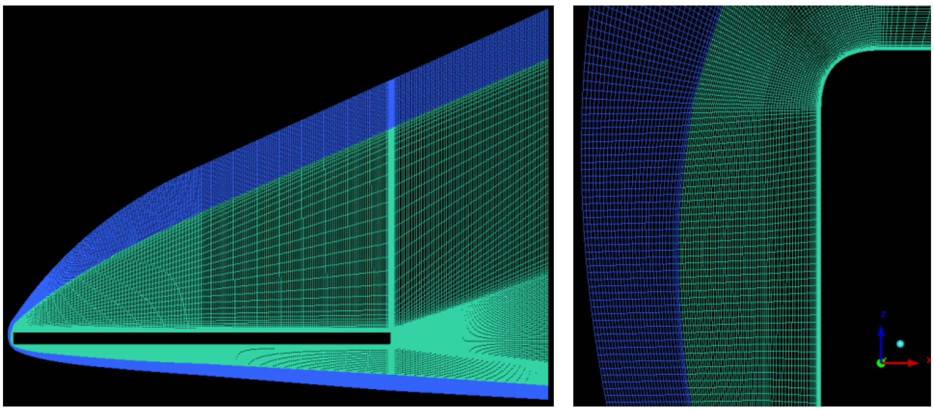

Figure 1. View of the mesh around a flat plate of 3m in length and 0.1 m in height.

DOI: 10.13009/EUCASS2017-603

3.1.2. Boundary conditions description

The geometry walls are considered as fully catalytic in most of simulations performed. So, all atomic species impacting the wall recombine. However, some complementary computations have been carried out assuming non-catalytic walls for different flight points. The wall catalycity characteristic depends on the material. For the sake of simplicity, we can say that metals and their alloys are rather catalytic while ceramics and composite materials are rather non-catalytic. Moreover, the wall temperature intensifies the wall catalytic power. The objective of these further computations is to define the maximal (obtained with a catalytic wall) and minimal (non-catalytic wall) heat flux received by the wall for the flight point considered. The rational followed in the present study is to avoid an overestimation of the heat flux received by the wall. The consequence in the case of space debris atmospheric re-entry will be an overestimation of the thermal degradation and thus an underestimation of the ground risk at final. The total (convective + diffusive) heat flux computed assuming a catalytic wall will be compared to the one obtained for a non-catalytic wall. The wall temperature can be fixed or computed assuming the radiative equilibrium. In this case, the wall emissivity is set at 0.8. The initial upstream conditions (velocity, pressure, temperature) are given by the flight point.

3.1.3. Computational parameters

CFD computations of given geometries have been conducted with the ONERA unstructured Navier-Stokes code CEDRE and using a chemical non-equilibrium model based on Park's kinetics to assume real gas effect occurring at high Mach numbers. However, the gas condition depends on the flight point, the form and the attitude of the object. So, according to these parameters, the flow computed by CEDRE can be locally a perfect gas or a real gas at thermochemical equilibrium or non-equilibrium. In other words, the gas condition is not then fixed by the user but by the environment itself.
The Navier-Stokes equations have been solved with a second-order finite-volume discretization in space, with the flux vector splitting AUSM+ or HLLC scheme associated to a Van Leer limiter. The time integration has been set to a one-step fully implicit approach. No turbulence model has been employed since laminar status of the flow is expected.

3.2. Analysis of the CFD database

The influence of the flight point, the size and the attitude of flat plates and boxes on the wall pressure and heat flux distributions (*conv*: convective; *tot*: convective + diffusive) is analyzed according to the location (X or Z) on the plate. The used coordinates system is sketched in Figure 2.

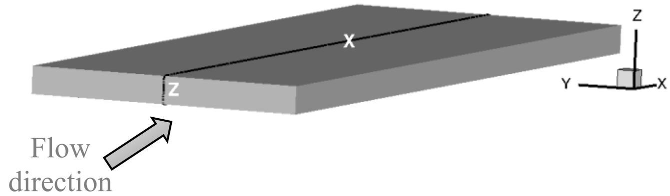

Figure 2. Coordinates system associated to the flat plate.

3.2.1. Influence of the plate attitude

The stagnation point position moves according to the angle of attack α. Located in the center of the flat plate for $\alpha = 0°$, it is situated just before the blunted edge for $\alpha = 25°$ (Figure 3.a). Beyond that incidence value, the stagnation point is located on the blunt edge of the flat plate (Figure 3.b). For $0° \leq \alpha < 45°$ and $45° \leq \alpha < 90°$, the sonic lines are fixed on the edges of the front face, as illustrated in Figure 4. So, one of the face is located in a flow compression zone while the other is situated in a flow expansion zone. The wall pressure and heat flux distributions are then different depending on whether the flat surface is in a compression or expansion flow area (Figure 5 and Figure 6). For $\alpha = 45°$, the shock shape changes significantly ; A normal shock instead of a curved shock wave appears as exhibited in Figure 3.b. The bow shock is almost attached. The compression zone is reduced to the neighborhood of the blunted edge of the plate and the two planar surfaces are located in expansion zone of the flow (Figure 3.b). So, for $\alpha = 45°$, the wall pressure and heat flux distributions are similar on the two faces (YZ and XY planes) of the plate (Figure 5 and Figure 6). In the expansion zone of the flow, the wall pressure is constant along the

DOI: 10.13009/EUCASS2017-603

plate while the wall heat flux decreases according to x direction. The wall pressure and heat flux distributions increase with angle of attack (Figure 5.b and Figure 6.b).
Finally, the position of the stagnation point does not correspond to the position of the maximal heat flux, which is around the blunt edge (Figure 6).

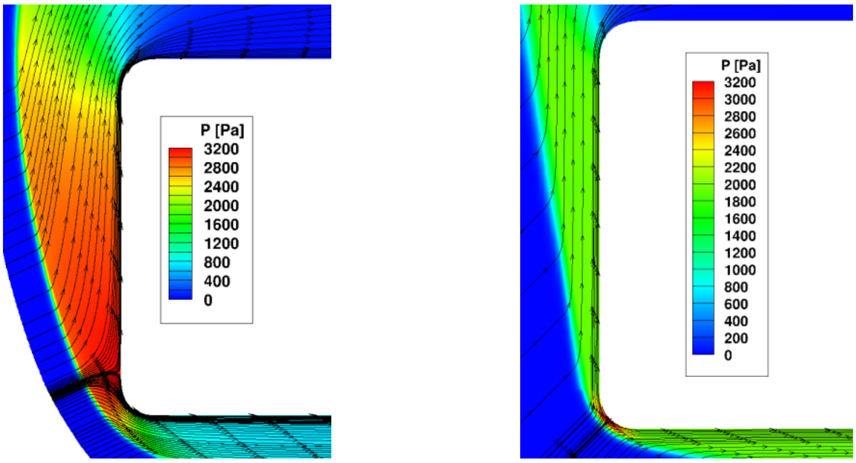

a) $\alpha = 25°$ *b)* $\alpha = 45°$

Figure 3. Pressure field and position of the stagnation point for 70 km, $V_\infty = 5959\ m/s$ and two angles of attack ($\alpha = 25°$ and $\alpha = 45°$).

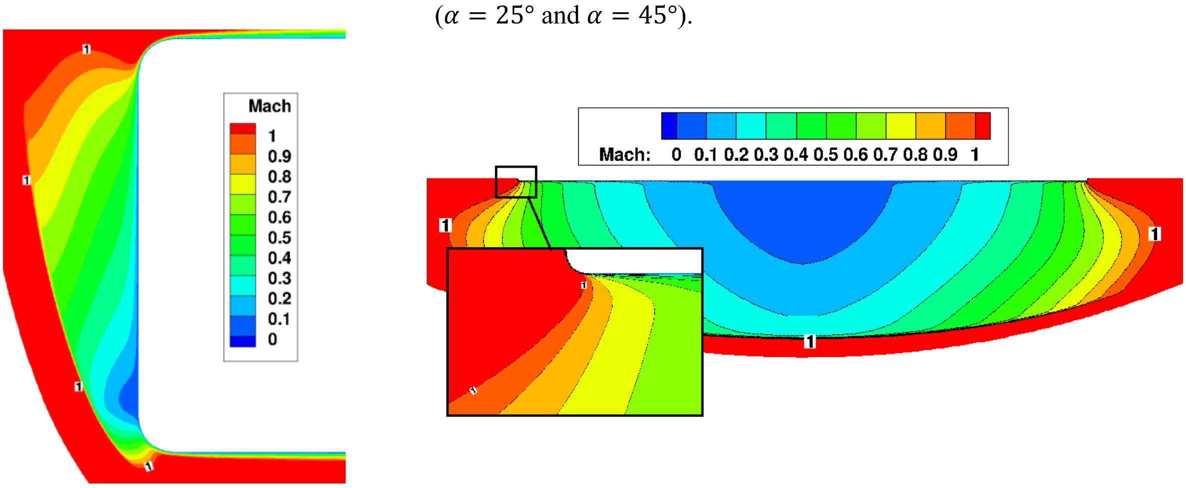

a) $\alpha = 25°$ *b)* $\alpha = 90°$

Figure 4. Location of the subsonic zone according to the angle of attack for 70 km, $V_\infty = 5959\ m/s$.

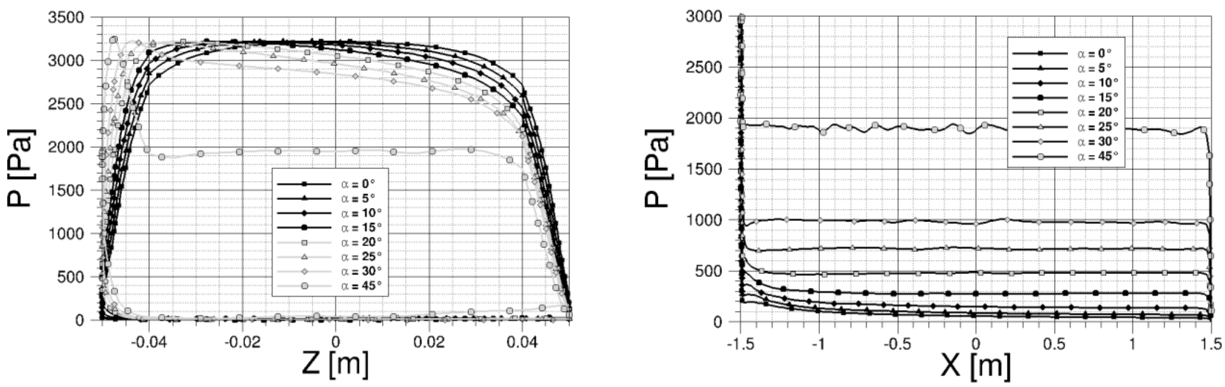

a) *b)*

Figure 5. Influence of angle of attack on the pressure distribution over a flat plate of 3 m in length (X) and 0.1 m in height (Z) for 70 km, $V_\infty = 5959\ m/s$.

DOI: 10.13009/EUCASS2017-603

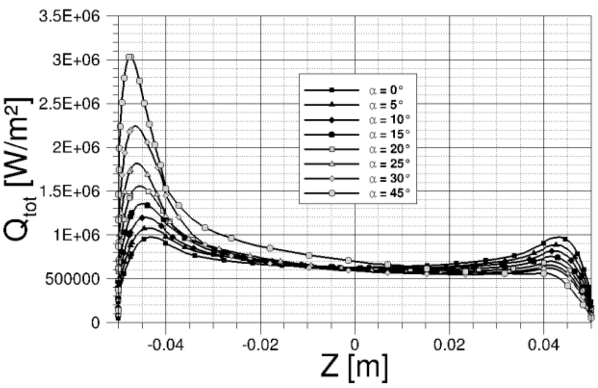

a)

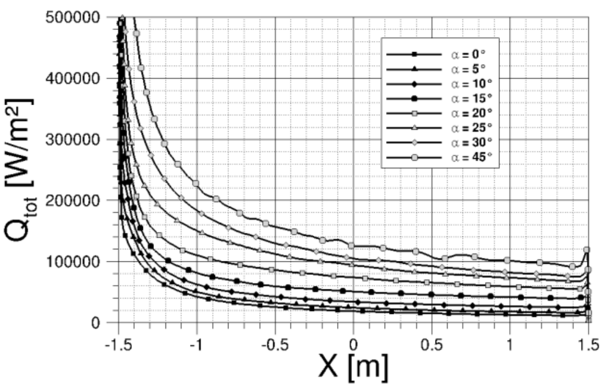

b)

Figure 6. Influence of angle of attack on the wall heat flux distribution over a flat plate of 3 m in length (X) and 0.1 m in height (Z) for $70\ km$, $V_\infty = 5959\ m/s$, in the case of a catalytic wall.

3.2.2. Influence of flight points

The wall pressure and heat flux distributions vary accordingly to the flight points: [70km, 5959 m/s], [58km, 4770 m/s], [50km, 4000 m/s], [40km, 2888 m/s]. Indeed, the flight point has a significant influence on the pressure distribution over the surface in compression and expansion zone of the flow (Figure 20).
For the flight point [40km, 2888 m/s], the flow is observed chemically frozen close to a perfect gas, while for the others flight points considered, the flow is in thermochemical equilibrium or non-equilibrium. For the face in an expansion flow (Figure 7.b), the influence of the flight point on the heat flux distribution is lower compared to the compression zone.

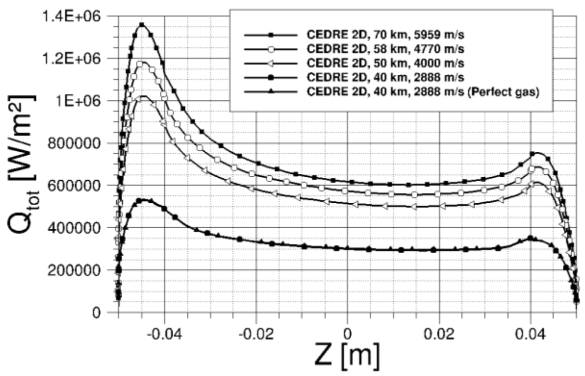

a)

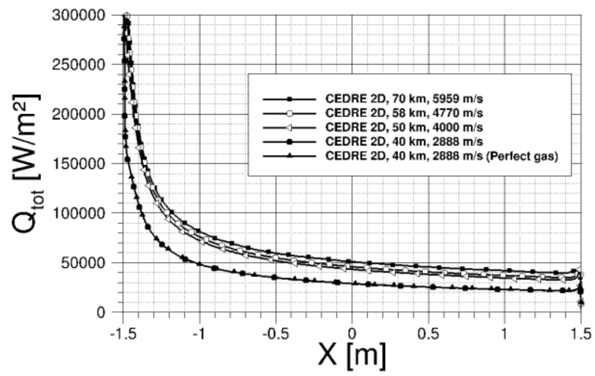

b)

Figure 7. Influence of the flight point (altitude, velocity) on the wall heat flux distribution along a flat plate of 3 m in length (X) and 0.1 m in height (Z) , in the case of a catalytic wall and for α = 15°.

3.2.3. Influence of size characteristics of the flat plate

For a flat plate of 3 m in length (X) and 0.1 m in height (Z), three edges curvature radius have been considered: $Rn = 0.005\ m$, $Rn = 0.01\ m$ et $Rn = 0.02\ m$ (Figure 8 and Figure 9). In addition, three lengths (L according to X) and two heights (h according to Z) have been studied (Figure 10 and Figure 11). Numerical simulations have been done for the flight point [70km, 5959 m/s] and for 15° of angle of attack.
The curvature radius of the flat plate edges has a limited influence on the pressure and heat flux distribution on the planar surface (Figure 8 and Figure 9). When the curvature radius of the blunt edges represents more than 40% of the considered length of the plate, the heat flux distribution on the planar surface is significantly affected.
The level of the pressure distribution on the planar surface located in a compression flow (subsonic zone around the stagnation point) is not influenced by the height of the plate (Figure 10.a) contrary to the level of the heat flux distribution (Figure 11.a). Finally, regarding the planar surface located in an expansion flow (supersonic zone), both the pressure and heat flux distributions decrease from the leading edge (Figure 10.b and Figure 11.b). In other words, the values of the wall pressure and heat flux at a specific location from the leading edge are identical whatever the total length of the flat plate is.

DOI: 10.13009/EUCASS2017-603

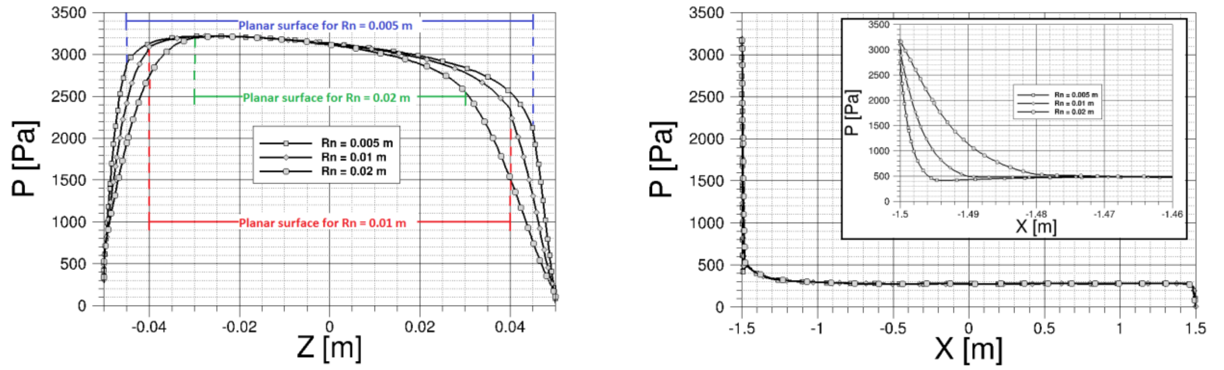

a) *b)*

Figure 8. Influence of the curvature radius of the plate edges on the wall pressure distribution along a flat plate of 3 m in length (X) and 0.1 m in height (Z), for the flight point [70 km, 5959 m/s, α = 15°].

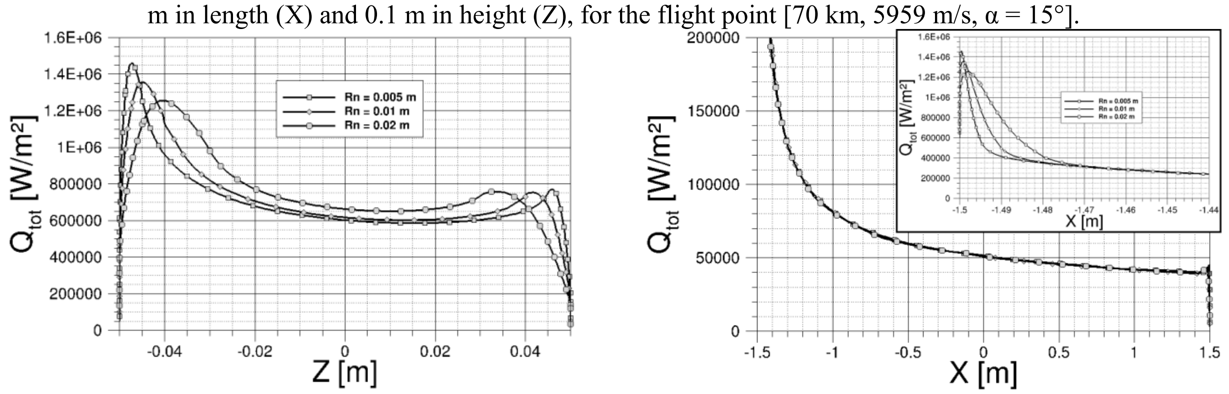

a) *b)*

Figure 9. Influence of the curvature radius of the plate edges on the wall heat flux distribution along a flat plate of 3 m in length (X) and 0.1 m in height (Z), for the flight point [70 km, 5959 m/s, α = 15°] and for a catalytic wall.

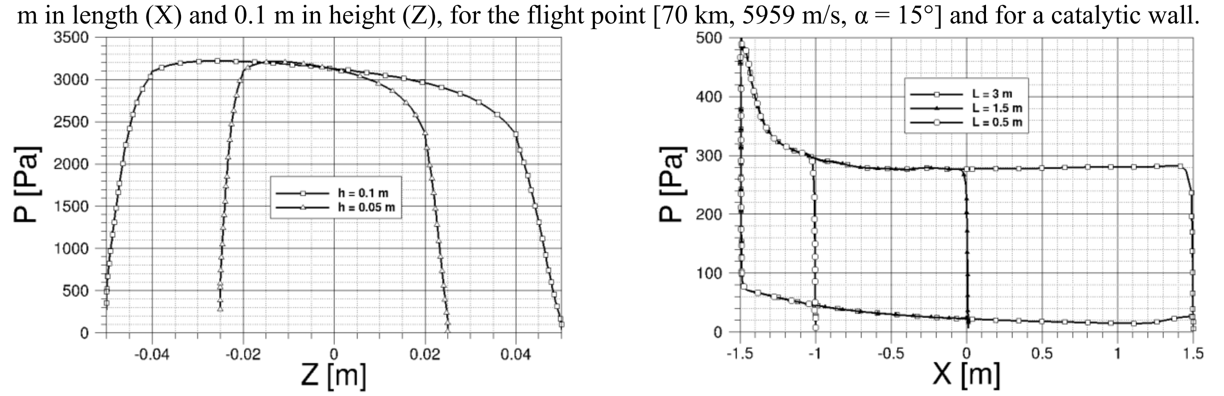

a) *b)*

Figure 10. Influence of the height and length of the plate on the pressure distribution along a flat plate of 3 m in length (X) and 0.1 m in height (Z), for the flight point [70 km, 5959 m/s, α = 15°].

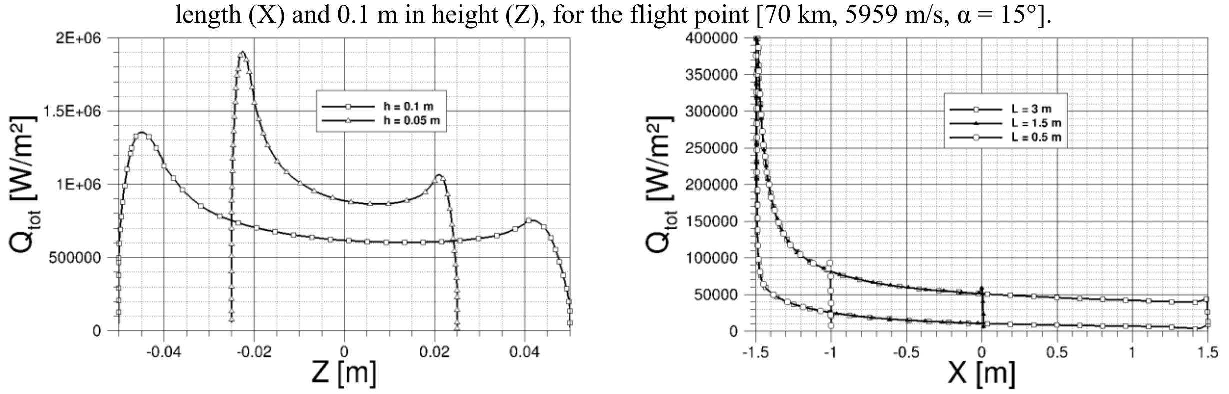

a) *b)*

Figure 11. Influence of the height and length of the plate on the heat flux distribution along a flat plate of 3 m in length (X) and 0.1 m in height (Z), for the flight point [70 km, 5959 m/s, α = 15°] and for a catalytic wall.

DOI: 10.13009/EUCASS2017-603

3.2.4. Influence of the wall catalycity

The influence of the wall catalycity on the wall heat flux distribution has been investigated for the flight points [70 km, 5959 m/s, $\alpha = 10°$], [58 km, 4770 m/s, $\alpha = 15°$] and [40 km, 2888 m/s, $\alpha = 15°$]. As shown in Figure 12.a (surface located in the subsonic zone around the stagnation point), whatever the flight point considered, total heat flux levels vary with the wall catalycity assumption. For higher flight points, the difference between heat fluxes for catalytic and non-catalytic wall is more significant. Indeed, higher upstream flow velocity at a given altitude induces more molecular dissociation in the shock layer and thus more recombination in the case of a catalytic wall. The difference between heat flux considering catalytic and non-catalytic walls reduces with increasing distance to the stagnation point (Figure 12.b).

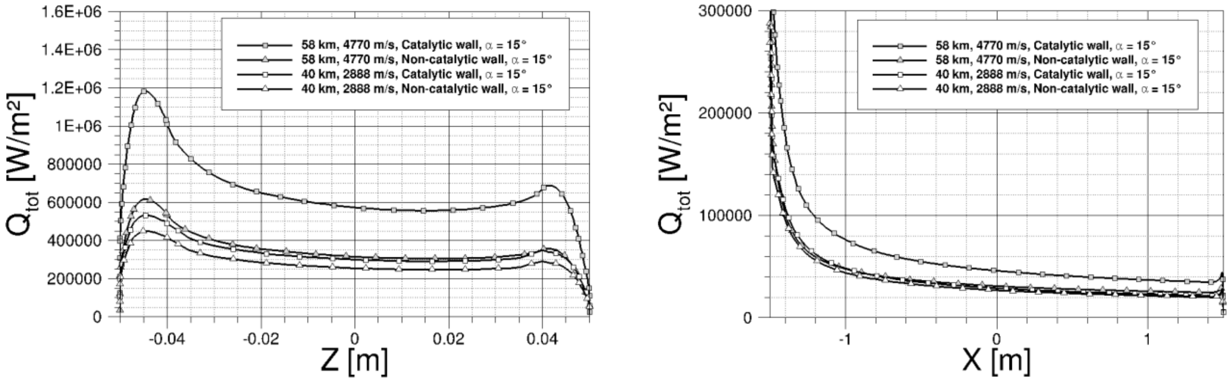

a) *b)*

Figure 12. Influence of the wall catalycity on the heat flux distribution along a flat plate of 3 m in length (X) and 0.1 m in height (Z), for various flight point and α = 15°.

4. The challenges

Formulations proposed in open literature or internally at CNES and ONERA in Spacecraft-Oriented codes for debris re-entry scenarios, such as PAMPERO and FAST/MUSIC respectively, are now evaluated by comparison with CEDRE numerical simulations. The objective is to evaluate the performance of the analytical models currently used and then to establish a statement to update them or not accordingly to “high fidelity” solutions from CFD databases. Such update could be directly to substitute present analytical expressions and/or correlations with former studies or/and develop new ones aiming at a better representation of CFD solutions.

4.1. Comparison of CFD to FAST/MUSIC and PAMPERO results

Therefore and as a first step, analytical (FAST/MUSIC and PAMPERO) and numerical (CEDRE) pressure and heat flux distributions are compared one another with regards to the attitude of the plate and the flight points (altitude, velocity).

4.1.1. Analysis of the wall pressure distribution

Numerical results of CEDRE code have been compared to the data obtained with FAST/MUSIC and PAMPERO for a flat plate of 3 m in length and 0.1 m in height, for several flight points and 4 angles of attack: $\alpha = 0°, 15°, 25°, 45°$. For the sake of simplicity, only solutions obtained for the flight point [70km, 5959 m/s] are exhibited.
For $\alpha = 0°$, the stagnation point pressure is lightly over-estimated by FAST/MUSIC (1.38%) and under-estimated by PAMPERO (3.49%) compared to CEDRE computational results (Figure 13.a et b). These disparities could have two visible sources: 1) a difference about the upstream conditions ($P_\infty; \rho_\infty; T_\infty; h_\infty$) due to a difference in the atmospheric model used in FAST/MUSIC and PAMPERO; 2) a difference about the Mollier diagram used to compute conditions behind the shock (for high enthalpy trajectory point, thermochemical is assumed for the gas flow).
In continuum regime, FAST/MUSIC and PAMPERO use timeless modified Newtonian model to compute the wall pressure distribution:

$$Cp = Cp_{stag} \times \sin^2 \theta \qquad (1)$$

Where Cp_{stag} is the pressure coefficient computed at stagnation point. θ is the angle between the velocity vector and the tangent to the mesh cell considered and is identical in each point of a planar surface.

DOI: 10.13009/EUCASS2017-603

So, the wall pressure distribution obtained with this model is identical and equal to the stagnation point pressure overall the surface facing the flow for $\alpha = 0°$. This is not fully representative of the physics of the flow, which is rather elliptical due to the presence of a large subsonic zone (cf. Figure 4 and Figure 13.a). The same remark can be done for $\alpha = 15°$ and $25°$. For $\alpha = 45°$, the pressure distribution on the blunted edge is well predicted by the modified Newtonian model due to a narrower subsonic zone. On the planar surface, the pressure distribution is constant. However, the pressure level is under-estimated by FAST (16%) and PAMPERO (20%).

For the surface in a flow expansion zone (Figure 13.c and d), the wall pressure levels are under-estimated by the Modified Newtonian model implemented in both FAST/MUSIC and PAMPERO, whatever the angle of attack is. The discrepancy with the CFD results is around 20% for $\alpha = 15°$, 19 % for $\alpha = 25°$ and 14 % for $\alpha = 45°$ (17 % for PAMPERO in this last case).

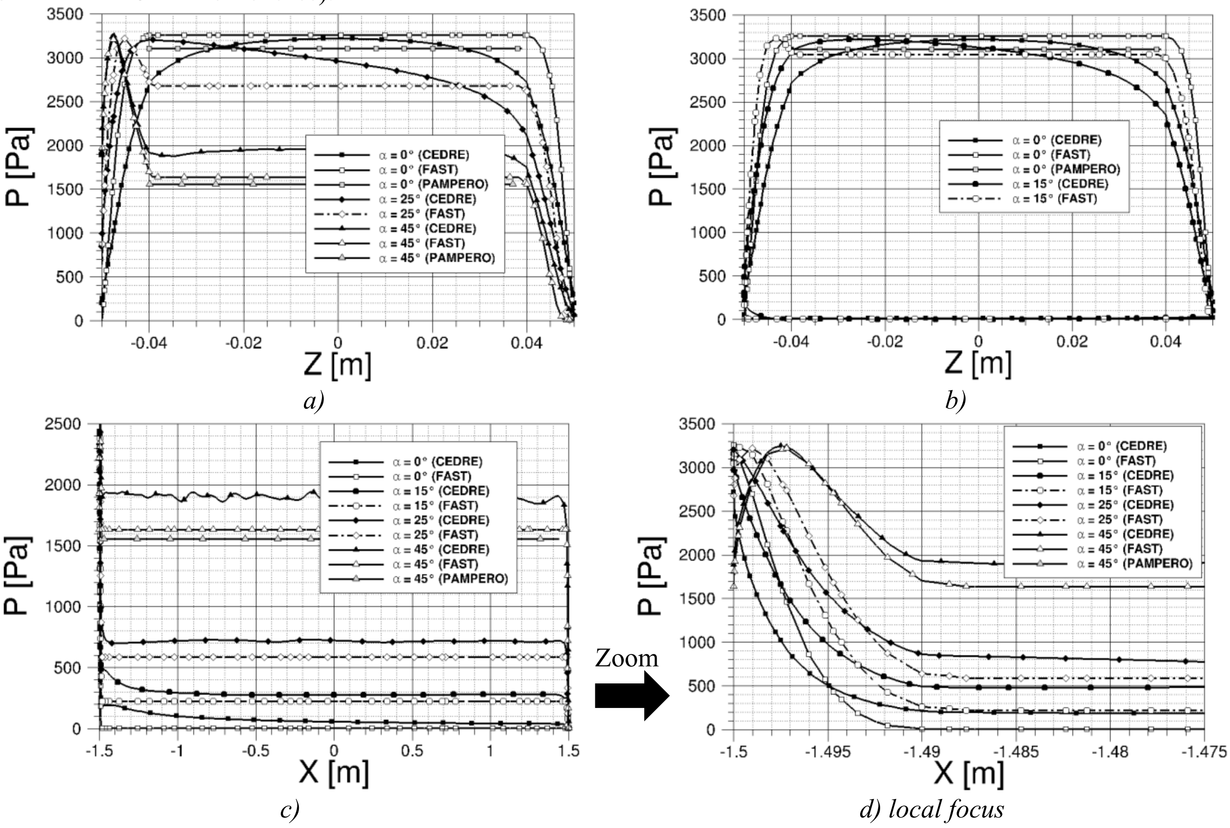

Figure 13. Comparison of pressure distributions according to Navier-Stokes (CEDRE) and analytical (FAST/MUSIC, PAMPERO) computations along a flat plate of 3 m in length (X) and 0.1 m in height (Z) for the flight point [70km, 5959 m/s] and $\alpha = 0°, 15°, 25°, 45°$ angles of attack.

4.1.2. Analysis of the wall heat flux distribution

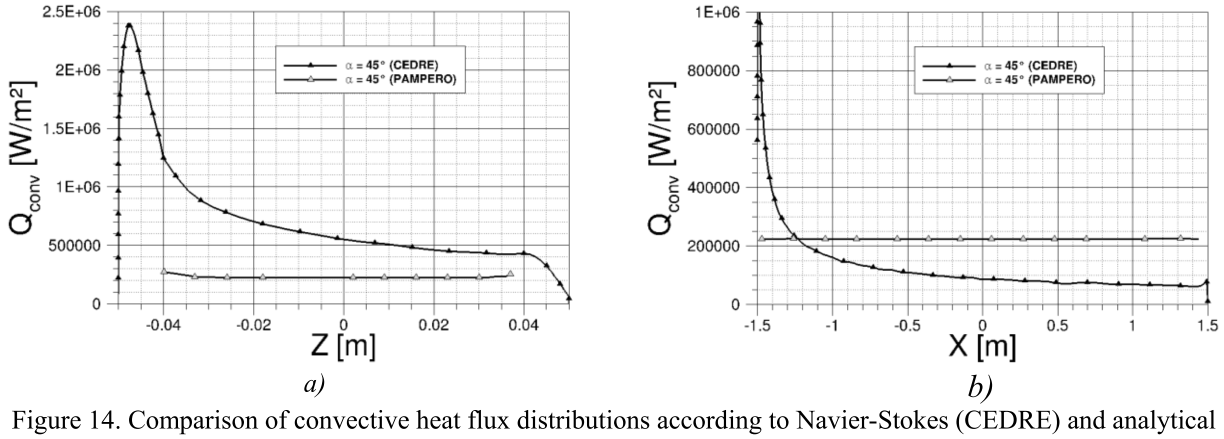

Figure 14. Comparison of convective heat flux distributions according to Navier-Stokes (CEDRE) and analytical (PAMPERO) computations along a flat plate of 3 m in length (X) and 0.1 m in height (Z) for the flight point [70 km, 5959 m/s, $\alpha = 45°$].

DOI: 10.13009/EUCASS2017-603

Due to a different strategy between PAMPERO and FAST/MUSIC to describe wall heat loads, PAMPERO results are firstly compared to the convective heat flux from CFD solutions with CEDRE (Figure 14 and Figure 15). Secondly, heating analytical solutions from FAST/MUSIC described by a wall total (convective + diffusive) heat flux distribution are confronted to CFD ones (Figure 16).

For $\alpha = 45°$ and the flight point [70km, 5959 m/s], the discrepancy between Navier-Stokes computations (CEDRE) and analytical solutions (PAMPERO) is noticed significant, between 0% and 311% (Figure 14). For $\alpha = 15°$, the discrepancy remains important between numerical and analytical convective heat flux distribution for the surface in the flow expansion zone (Figure 15.a). However, for the surface in the flow compression zone (Figure 15.b), the convective heat flux seems well predicted by PAMPERO. A mean difference of 12% is noted for the flight point [60 km, 5459 m/s, $\alpha = 15°$]. For the flight point [70 km, 5459 m/s, $\alpha = 15°$], the discrepancy is almost zero near the trailing edge and reaches 30% near the leading edge (Figure 15.b).

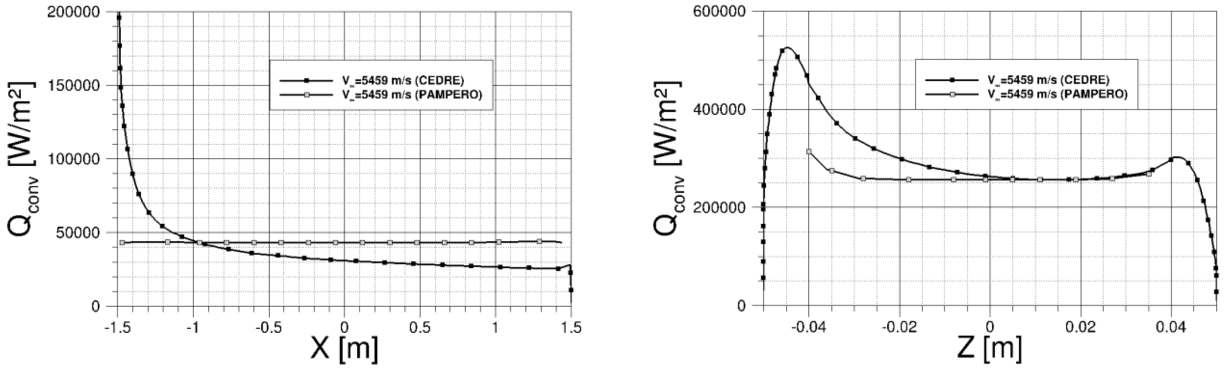

a) *b)*

Figure 15. Comparison of convective heat flux distributions according to Navier-Stokes (CEDRE) and analytical (PAMPERO) computations along a flat plate of 3 m in length and 0.1 m in height for the flight point [70 km, 5459 m/s, $\alpha = 15°$]

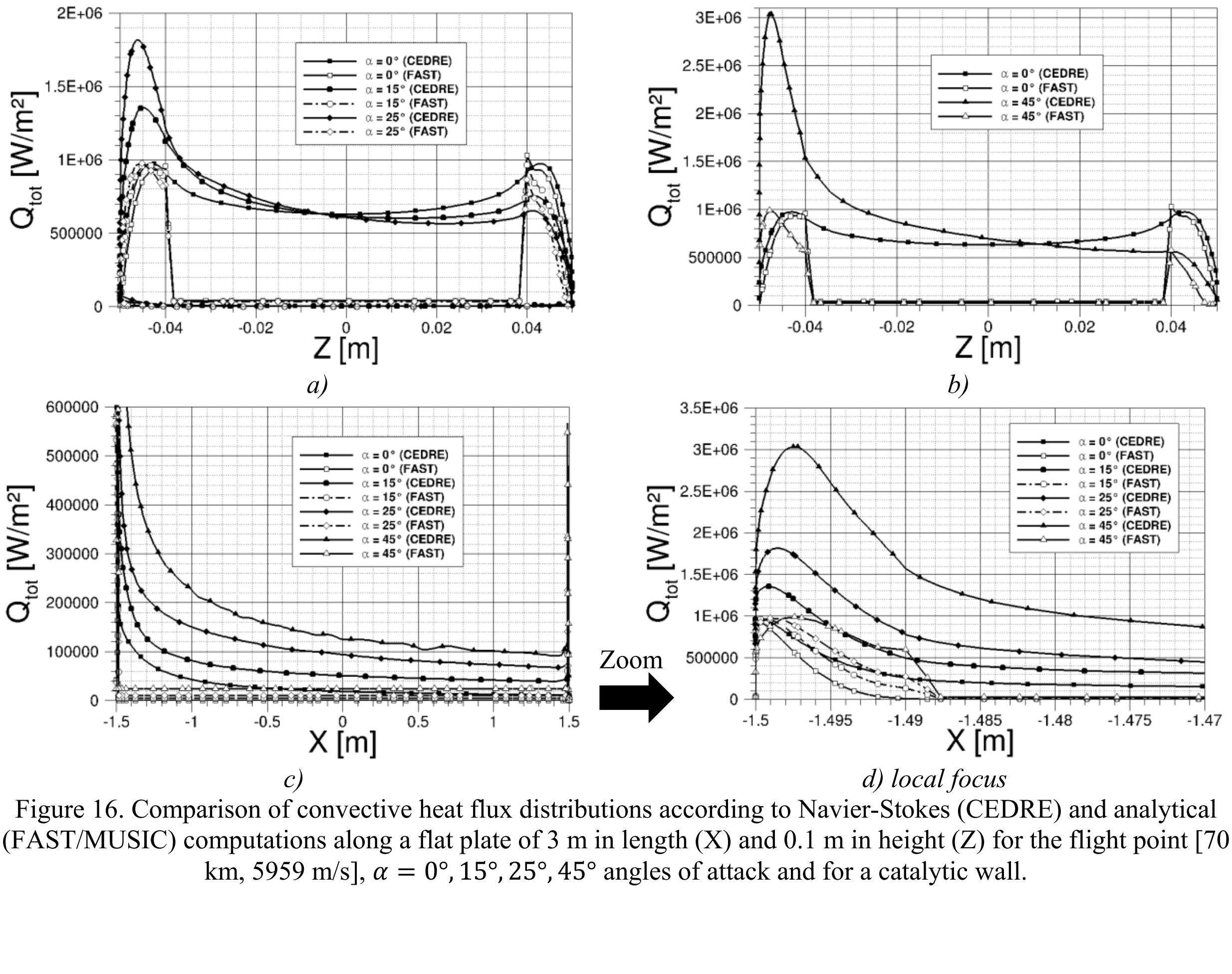

a) *b)*

c) *d) local focus*

Figure 16. Comparison of convective heat flux distributions according to Navier-Stokes (CEDRE) and analytical (FAST/MUSIC) computations along a flat plate of 3 m in length (X) and 0.1 m in height (Z) for the flight point [70 km, 5959 m/s], $\alpha = 0°, 15°, 25°, 45°$ angles of attack and for a catalytic wall.

DOI: 10.13009/EUCASS2017-603

The wall heat flux model implemented in FAST/MUSIC is inversely proportional to the square root of the local curvature radius. For a flat plate, the local curvature radius approaching infinity, the total heat flux approaches zero, as shown in Figure 16. For $\alpha = 0°$, the total heat flux distribution on the blunted edge ($Rn = 0.01\ m$) is correctly predicted by FAST/MUSIC (Figure 16). However, the model cannot predict the increase of the wall heat flux on the blunted edge with the increase of the angle of attack. It is obvious that an important update is expected for planar areas since a representative total heating model cannot be directly described by an inverse function of the local curvature radius. Even though PAMPERO convective heating model is sometimes less affected by surface local curvature, discrepancies remain noticeable whatever flight conditions tested.

4.2. Comparison CFD results with literature model

Amid many literature models, very few can be applied simply in spacecraft oriented tools for which 2D or 3D local models are needed. Those that appeared the most relevant ones after a broad bibliography are presented here. Correlations developed in the 1950s – 1960s are often based on the resolution of the boundary layer equations. One of the most famous correlations is the Eckert reference temperature, also called reference enthalpy. With this approach, the heat transfer rate is computed using the relations developed for the incompressible flows where the parameters depending on the temperature are evaluated to the Eckert reference temperature.
Hankey *et al.* [27] proposed a practical expression for flat plate in hypersonic regime with angle of attack (α) and attached oblique shock for laminar or turbulent boundary layer. In laminar flow regime:

$$q_{tot} = 6879\ \frac{\alpha^{2/3}}{x^{1/2}} \left(\frac{\rho_\infty}{\rho_0}\right)^{\frac{1}{2}} \left(\frac{V_\infty}{10^3}\right)^3 \left(1 - \frac{h_w}{H}\right) \tag{2}$$

where q_{tot} is the total heat flux received by the wall, including convective and diffusive terms (W/m^2). α is the angle of attack ($deg.$), x the distance from the leading edge (m), ρ the density (kg/m^3), V the velocity (m/s), h_w the wall enthalpy (J/kg) and H the total enthalpy (J/kg). Subscripts 0 and ∞ refer to the conditions at sea level and upstream shock conditions at the considered altitude respectively.

Equation (2), depending mainly on upstream conditions as well as on the total and wall enthalpies, can be easily applied. However, according to [27] equation 2 can be used for $\alpha > 5°$ only. For smaller angles of attack, Gilly *et al.*[19] proposed the following alternative equation for laminar flows:

$$q_{tot} = 0.51 \times 10^{-4}\ V_\infty^{2.12} \frac{1}{x^{\frac{1}{2}}} p_\infty^{\frac{1}{2}} (\cos\alpha)^{\frac{1}{2}} \left(1 - \frac{2\,h_w}{V_\infty^2}\right) \sqrt{1 + 1.45(\sin\alpha)^{1.8}\, M_\infty} \tag{3}$$

The first objective is to determine if the proposed equations are also applicable when the shock is detached (strong shock). Moreover, equations 2 and 3 have been obtained assuming an ideal equivalent gas to get an analogy for shock layer with real gas effect by setting $\gamma = 1.2$. So, the second objective is to verify if equation (2) can be applicable for other values of γ. The values of γ near the wall (computed by CEDRE for given flight point [70km, 5959 m/s] in the case where the wall temperature is fixed and chemical non-equilibrium assumed) are displayed in Table 1.

Flight points [70km, 5959 m/s]				
$T_w = 200\ K$	$T_w = 700\ K$	$T_w = 1000\ K$	$T_w = 1500\ K$	$T_w = 2000\ K$
$\gamma_{CL} = 1.4$	$\gamma_{CL} = 1.36$	$\gamma_{CL} = 1.34$	$\gamma_{CL} = 1.32$	$\gamma_{CL} = 1.3$

Table 1. CFD computed value of the specific heat ratio near the wall according to the wall temperature.

For all the cases presented in Table 1 heat flux distribution obtained by Hankey model is compared to Navier-Stokes solution in Figure 17. As observed in Figure 17, Hankey formulation (Eq. 2) describes properly the total heat flux distribution $\left(Ch_{tot} = \frac{Q_{tot}}{\frac{1}{2}\rho_\infty V_\infty^3}\right)$ for a surface in a flow expansion zone even if the shock is a detached shock. As noticed, the specific heat ratio γ has not a significant influence on the heat flux distribution along the flat plate with a significant length (in Figure 17, L = 3 m).

DOI: 10.13009/EUCASS2017-603

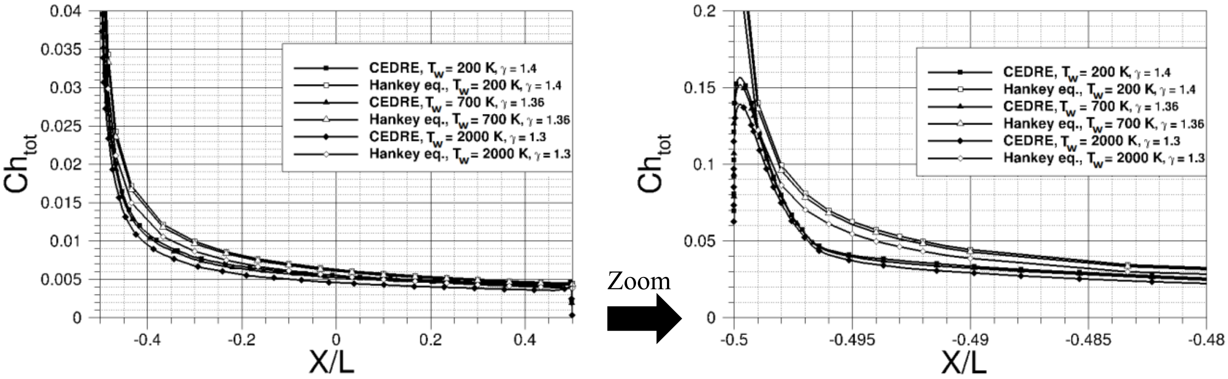

a) *b) local focus*

Figure 17. Comparison of numerical (CEDRE) and analytical (Hankey, Eq. 2) heat flux coefficient distribution in laminar regime along a flat plate of 3 m in length (X) and 0.1 m in height (Z) for the given flight point [70 km, 5959 m/s, α = 15°] and a catalytic wall.

5. Development and validation of the new analytical models

Formulations proposed internally at CNES and ONERA have highlighted a disparity or a weak performance compared to CFD data. In open literature, only Hankey *et al.* [27] correlation can be used and implemented in Spacecraft Oriented codes. However, its application is dedicated to the wall heat flux distribution along a planar surface in an expansion flow. Therefore, ONERA has developed new analytical models for the pressure (surfaces in compression and expansion flows) and heat flux distributions (for surface in compression flow only) on flat plate types. Only the total heat flux distribution for a catalytic wall has been modeled since no heating models can be generalized for the convective heat flux or for the non-catalytic wall property. The validation of the new models is then discussed in this paragraph.

5.1. Validation of models for the prediction of the wall pressure distribution

The new models developed for the pressure distribution are now evaluated for several flight points, flat plate attitudes (angles of attack) and sizes (length, height, edge curvature radius).

5.1.1. Influence of the attitude of the flat plate

The wall pressure distribution is well predicted by the new analytical model when the surface is in the expanded flow zone (Figure 18), whatever the angle of attack is. The wall pressure on the planar surface ($-0.495 \leq x/L \leq 0.495$) is predicted by the model with an accuracy between 0.3% and 4% according to the angle of attack.

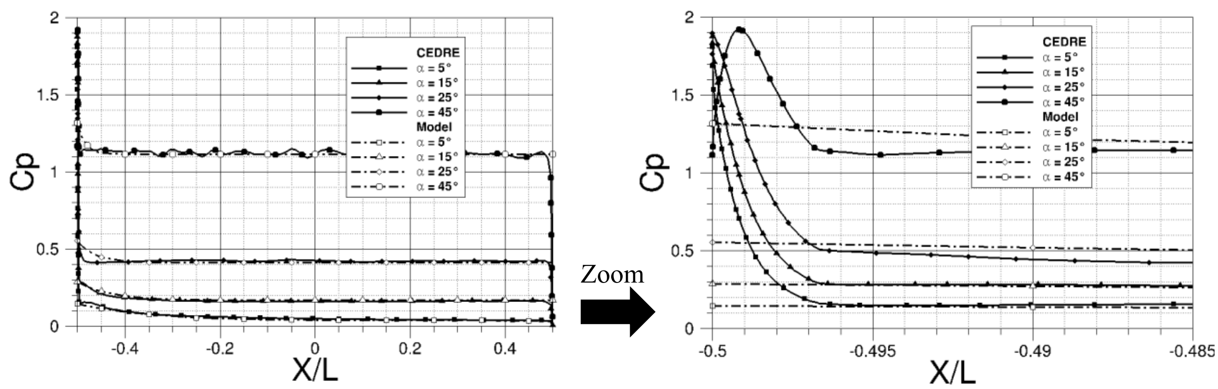

a) *b)local focus*

Figure 18. Comparison of pressure distribution according to Navier-Stokes (CEDRE) and new analytical model developed along a flat plate of 3 m in length (X) and 0.1 m in height (Z) for the flight point [70 km, 5959 m/s], and $\alpha = 0°, 10°, 20°\ and\ 30°$, with $L = 3\ m$ (according to X in Figure 2).

DOI: 10.13009/EUCASS2017-603

The new analytical model also describes correctly the wall pressure distribution for a surface in flow compression zone (Figure 19). The maximal discrepancy between the numerical and analytical results is between 0% and 7%. Increasing discrepancy follows increasing incidence.

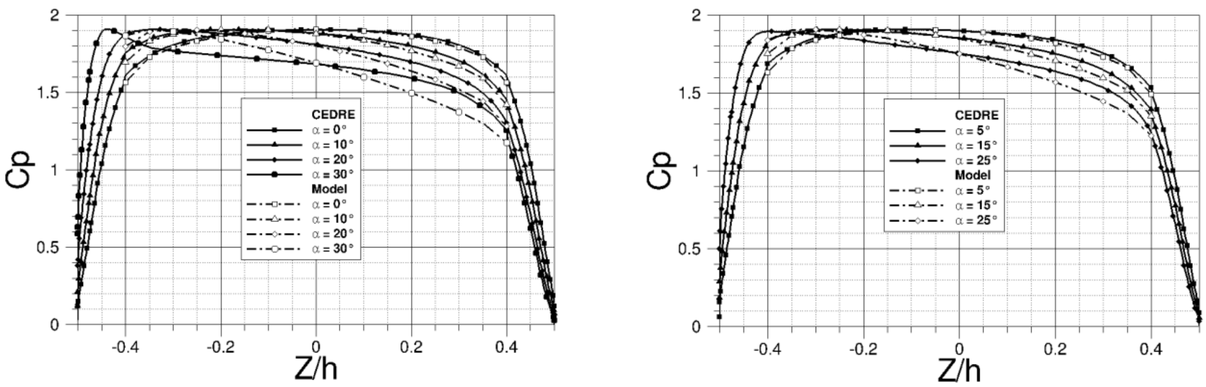

a) *b)*

Figure 19. Comparison of pressure distribution according to Navier-Stokes (CEDRE) and new analytical model developed along a flat plate of 3 m in length (X) and 0.1 m in height (Z) for the flight point [70 km, 5959 m/s] and $\alpha = 0°, 5°, 10°, 15°, 20°, 25°, 30°$ with $h = 0.1\ m$.

5.1.2. Influence of the flight point (altitude, velocity)

The comparison between the numerical and analytical results is satisfactory (Figure 20). A discrepancy of around 4% is noticed for flight point influence surprisingly for lowest altitude (2888m/s) and weaker real gas effects.

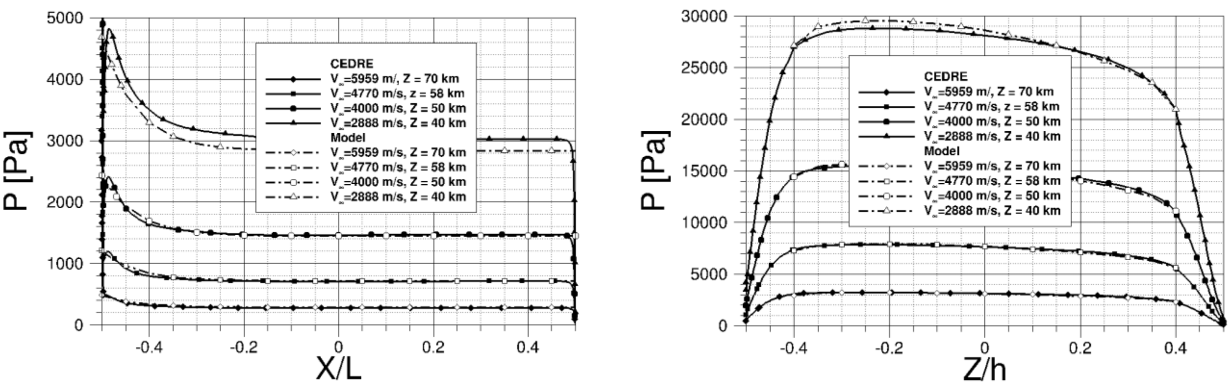

a) L = 3 m *b) h = 0.1 m*

Figure 20. Comparison of pressure distribution according to Navier-Stokes (CEDRE) and new analytical model developed along a flat plate of 3 m in length (X) and 0.1 m in height (Z) considering several flight points with α = 15°.

5.1.3. Influence of the geometrical characteristic of the plate

The influence of the curvature radius (Rn) of the blunted edges and the sizes of the flat plate (according to X and Z) are tested independently. In Figure 21.a, the pressure distribution obtained with the new analytical model is successfully compared to the numerical data from CEDRE along a flat plate of 3 m in length (X) and 0.1 m in height (Z) for the flight point [70 km, 5959 m/s] assuming three edge curvature radii: $Rn = 0.005\ m$, $Rn = 0.01\ m$ et $Rn = 0.02\ m$. In Figure 21.b, the edge curvature radius is fixed to 0.01 m while the height of the plate is successively modified: $h = 0.1\ m$ and h$= 3\ m$.

Whatever the edges curvature radius is, accuracy of the new model developed is noticed satisfying. However, for $Rn/h = 0.2$, i.e. when the curvature represents around 50% of the plate height, the model becomes weaker nearby the edges to represent planar flow.

DOI: 10.13009/EUCASS2017-603

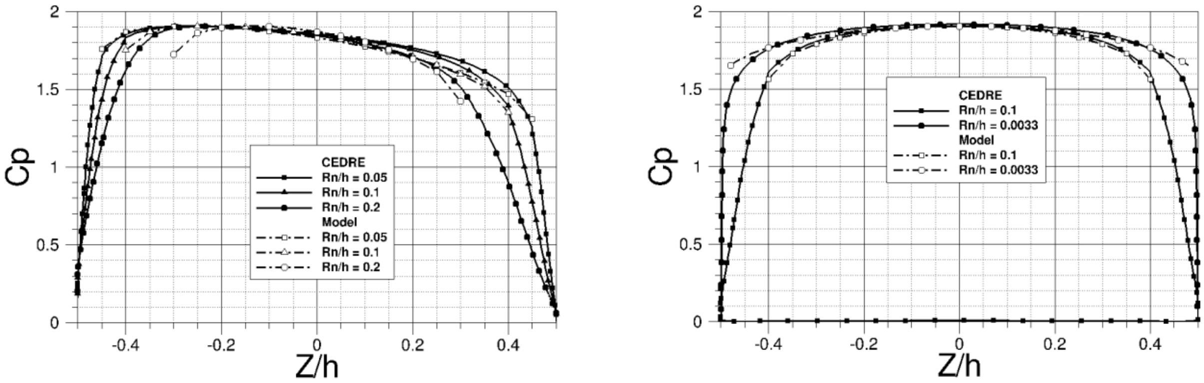

a) *Sensitivity of Rn with h = 0.1 m (α = 15°)* b) *Sensitivity of h with Rn = 0.01 m (α = 0°)*

Figure 21. Comparison of pressure distribution according to Navier-Stokes (CEDRE) and new analytical model developed along a flat plate of 3 m in length (X) and 0.1 m or 3 m in height (Z) for the flight point [70 km, 5959 m/s] for several ratio Rn/h.

Finally, the pressure distribution along the planar surface in flow expansion zone does not change with the length of the planar surface (Figure 22). The new model developed is properly applicable for arbitrary surface lengths.

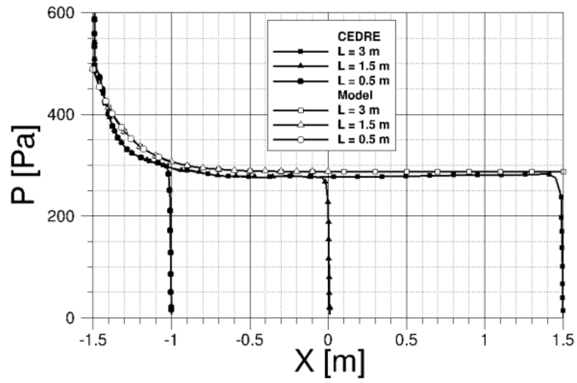

Figure 22. Comparison of pressure distribution according to Navier-Stokes (CEDRE) and new analytical model developed along a flat plate of 0.1 m in height, for several surface lengths L and for the given flight point [70km, 5959 m/s, α = 15°].

5.2. Validation of the wall heat flux distribution model

The new model developed by ONERA is dedicated to be applied to the surface in the flow compression zone, while Hankey *et al.* [27] model is used to describe the total heat flux (convective + diffusive heat flux) at the surface in the flow expansion zone.

5.2.1. Influence of the flight point (altitude, velocity)

The total wall heat flux distributions obtained with the new model are compared to CFD data from CEDRE in Figure 23 for several flight points along a flat plate of 3 m in length and 0.1 m in height and 15° angle of attack. The total heat flux obtained with the new analytical model is analogue with those of CFD results. For a surface in flow compression zone, accuracy of the model depends on the flight point. Indeed, for [70km, 5959 m/s] the relative error is between 1% and 18% (near the trailing edge) with a mean error around 5%. For the flight point [58km, 4770 m/s], the relative error is between 0.1% and 12.7% (around the trailing edge). For [40km, 2888 m/s], where the flow is frozen, analytical results present a greater mean error of about 15%. These observations are in opposite to what was noticed for the pressure distribution i.e larger discrepancy with CFD while decreasing altitude.

DOI: 10.13009/EUCASS2017-603

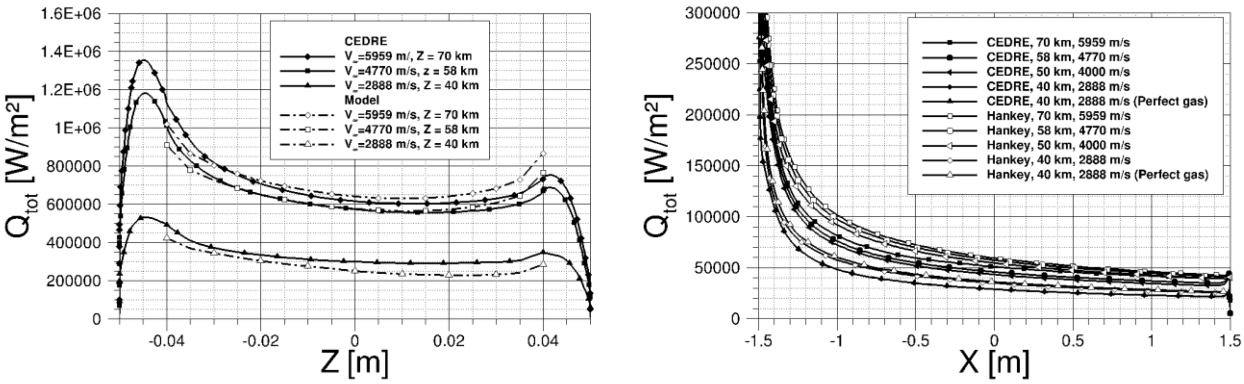

ONERA new analytical model *b) Hankey model*

Figure 23. Comparison of the total heat flux distribution according to Navier-Stokes (CEDRE) and analytical models along a flat plate of 3 m in length (X) and 0.1 m or 3 m in height (Z) considering several flight points with α = 15°, and a catalytic wall.

5.2.2. Influence of the attitude of the plate

The wall heat flux distributions obtained with the analytical models (ONERA correlation and Hankey *et al.* formulation) are confronted to CFD data from CEDRE in Figure 24 along a flat plate of 3 m length (L according to X) and 0.1 m height (h according to Z), for the highest altitude flight point and several angles of attack. The coordinates system associated to the flat plate is plotted in Figure 2.

The analytical results obtained with the new ONERA model (Figure 24.a) and with the Hankey model (Figure 24.b) are in quite good agreement with CFD results for any angle of attack. When the surface faces a flow compression zone (Figure 24.a), accuracy of the new model varies with the angle of attack. So, for $\alpha = 0°$, the relative error is between 3% and 7% with a mean error around 4%. For $\alpha = 15°$, the relative error varies between 0.9% and 18% (the maximal error is reached around the trailing edge), with a mean error around 5%. Finally, for $\alpha = 30°$, the relative error is between 2.5% and 29% (maximum error around the trailing edge), with a mean error around 6.5%.

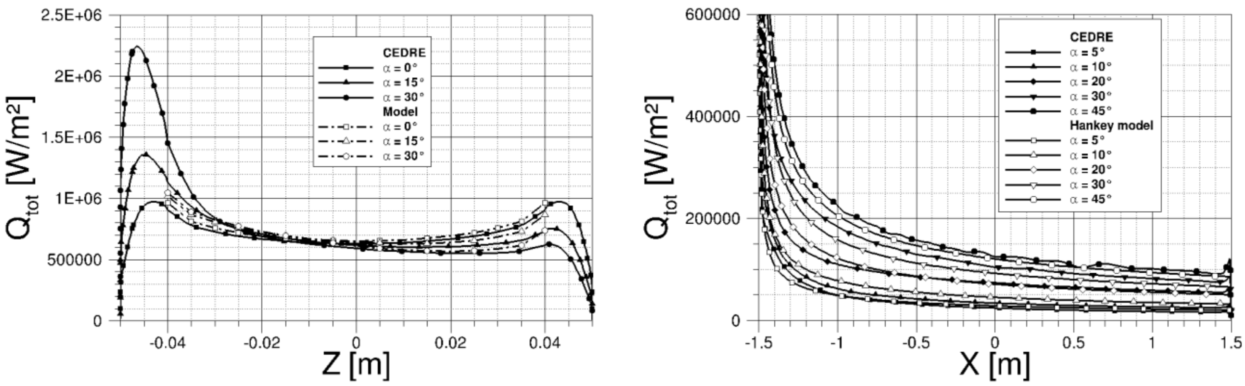

a) New ONERA analytical model b) *Hankey model*

Figure 24. Comparison of the total heat flux distribution according to Navier-Stokes (CEDRE) and analytical models along a flat plate of 3 m in length (X) and 0.1 m or 3 m in height (Z) for the given flight point [70 km, 5959 m/s], Rn = 0.01 m, ($\alpha = 0°, 5°, 10°, 15°, 20°, 30°, 45°$) angles of attack and a catalytic wall.

Angle of attack	Min. relative error	Max. relative error
5°	0.085%	27.4%
10°	0.45%	33.1%
20°	0.05%	22.4%
30°	0.16%	12.3%
45°	0.15%	9.3%

Tableau 1. Relative error (%) between Navier-Stokes (CEDRE) and Hankey model (Eq. 2) for the wall heat flux distribution according to the angle of attack for a flat surface in a flow expansion zone, for the given flight point [70km, 5959 m/s] and a catalytic wall.

DOI: 10.13009/EUCASS2017-603

For the surface in the flow expansion zone (Figure 24.b), the relative uncertainty induced by the Hankey model (Eq. 2) is precised in Tableau 1 according to the angle of attack. The maximum uncertainty is found in the vicinity of the leading edge. The Hankey model is more accurate for the angles of attack between 30° and 45°. This is not surprising since this model have been elaborated for thin flat plates where an attached shock is developed, which is almost the case for $\alpha = 45°$.

5.2.3. Influence of the geometrical characteristics of the flat plate

The plate sizes are the same as those considered in section 5.1.3. The analytical correlations (new ONERA model and Hankey formulation) are highly comparable with the CFD results for all the considered geometries of the flat plate, as plotted in Figure 25.

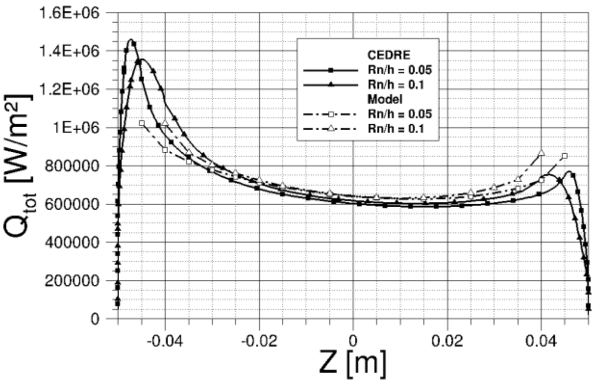

New ONERA analytical model

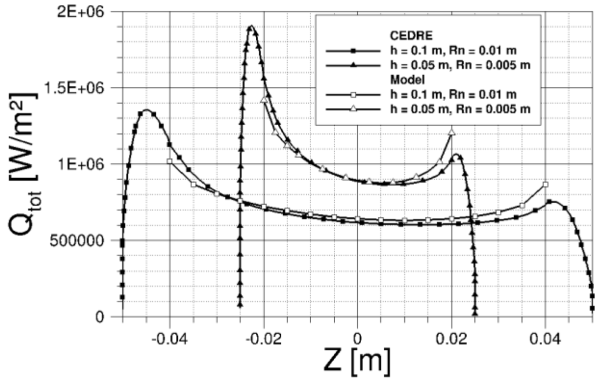

New ONERA analytical model

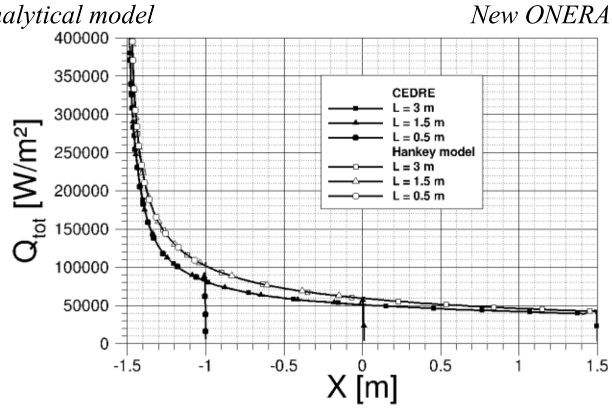

Hankey model

Figure 25. Comparison of the total heat flux distribution according to Navier-Stokes (CEDRE) and analytical models for various geometrical characteristics of the plate (length, height, curvature radius of the edges), for the given flight point [70 km, 5959 m/s, α = 15°].

6. Conclusion

Around 75 Navier-Stokes 2D/3D numerical simulations have been performed with the ONERA Navier-Stokes code CEDRE in order to develop an updated numerical database dedicated to ATD processes occurring on flat plates and boxes representing debris. An analysis of the database has been done to identify the key parameters influencing the wall pressure and heat flux distributions in terms of form and level.

Usual analytical models from open literature or those previously implemented in both FAST/MUSIC and PAMPERO engineering codes exhibited their weakness to describe properly wall pressure and wall heating in any conditions of re-entry debris flight. The Hankey correlation has been retained to describe the total heat flux distribution along a planar surface in a flow expansion zone while complementary new models have been developed and successfully compared to CFD results for both pressure and heat flux distributions. The accuracy of these models has been properly estimated according to flight point conditions, attitude and geometrical characteristics as piloting ATD processes. Obtained results led to significant improvements compared to previous models implemented in engineering codes to simulate planar surface debris re-entry.

Acknowledgments

These researches have received funding from CNES LOS program (French Space Law) as part of a Mutual Interest Project between CNES and ONERA related to atmospheric re-entry of space debris. We deeply thank Mr. Pierre Omaly, CNES LOS responsible, to have supported and funded present studies.

References

[1] H. Klinkrad. 2006. Space Debris: Models and Risk Analysis. Springer-Verlag, Berlin, Heidelberg.
[2] ESA. 2017. Space operation, Space debris: the ESA approach. ESA Space Debris brochure 2017.
[3] W. Ailor, W. Hallman, G. Steckel, M. Weaver. 2005. Analysis of reentered debris and implications for survivability modelling. In: *4th European Conference on Space Debris*.
[4] N.L. Johnson. 2001. Space debris modeling at NASA. In: *3rd European Conference on Space Debris*.
[5] T. Lips, B. Fritsche. 2005. A comparison of commonly used re-entry analysis tools. *Acta Astonautica*, 57: 312-323.
[6] C. Martin, C. Brandmueller, K. Bunte, J. Cheese, B. Fritsche, H. Klinkrad, T. Lips, N. Sanchez. 2005. A debris risk assessment tool supporting mitigation guidelines. In: *4th European Conference on Space Debris*.
[7] P. Omaly, C. Magnin-Vella, S. Galera. 2013. DEBRISK, CNES tool for re-entry survivability prediction: validation and sensitivity analysis. In: *6th IAASS Conference*.
[8] Z. Wu, R. Hu, X. Qu, X. Wang, Z. Wu. 2011. Space Debris Reentry Analysis Methods and Tools. *Chinese Journal of Aeronautics*, 24:387-395.
[9] G. Ortega, A. Blasco, S. Weikert. 2008. Space safety trajectory optimization and debris analysis using ASTOS at ESA. In: *37th COSPAR Scientific Assembly*.
[10] H-S. Sim, K-H. Kim. 2011. Reentry survival analysis of tumbling metallic hollow cylinder. *Advances in Space Research*, 48:914-922.
[11] T. Lips, B. Fritsche, M. Homeister, G. Koppenwallner, H. Klinkrad, M. Toussaint. 2007. Re-entry Risk Assessment for Launchers – Development of the New SCARAB 3.1L. In: *2nd IAASS Conference*.
[12] J. Annaloro, P. Omaly, V. Rivola, M. Spel. 2014. Elaboration of a New Spacecraft-Oriented Tool: PAMPERO. In: *8th European Symposium on Aerothermodynamics for Space Vehicles*.
[13] Y. Prévereaud, J.-L. Vérant, M. Balat-Pichelin, J.-M. Moschetta. 2016. Numerical and experimental study of the thermal degradation process during the atmospheric re-entry of a $TiAl_6V_4$ tank. *Acta Astonautica*, 122: 258-286.
[14] T. Lips. 2013. Equivalent Re-entry Breakup Altitude and Fragment List. In: *6th European Conference on Space Debris*.
[15] P.B. Burbank, R.L. Stallings. 1959. Heat-Transfer and Pressure Measurements on a Flat-Fasce Cylinder at a Mach number Range of 2.49 to 4.44. NASA Report TM X-221.
[16] T. Barth. 2008. Aero- and Thermodynamic Analysis to SHEFEX I. *Engineering Applications of Computational Fluid Mechanics*. 2:76-84.
[17] T.Barth, J.Longo. 2010. Advanced Aerothermodynamic analysis of SHEFEX I. *Aerospace Science and Technology*. 8:587-593.
[18] T. Barth, T. Eggers. 2007. SHEFEX – A First Aerodynamic Post-flight Analysis. *New Results in Numerical and Experimental Fluid Mechanics VI*. 96:291-299.
[19] L.P. Gilly, L. Rosenthal, Y. Sémézis. 1970. Aerodynamique Hypersonique. Gauthier-Villars Editeur, Paris.
[20] W.D. Hayes, R.F. Probstein. 1962. Hypersonic Flow Theory. Academic Press, New York-London.
[21] A.G. Hammitt, S.M. Bogdonoff. 1956. Hypersonic study of the leading edge effect on the flow over a flat plate. *Journal of Jet Propulsion*. 26:241-246
[22] G.G. Chernyi. 1961. Transition to Hypersonic Flow. Academic Press, New York.
[23] A. Sakurai. 1953. On the propagation and structure of the blast wave, I and II. *Journal of the Physical Society of Japan*. 2:256-266.
[24] D.L. Baradell, M.H. Bertram. 1960. The Blunt Plate in Hypersonic Flow. NASA Report. NASA TN-D-408.
[25] M.H. Bertram, D.L. Baradell. 1957. A Note on the Sonic-Wedge Leading Edge Approximation in Hypersonic Flow. *Journal of the Aeronautical Sciences*. 8:627-629.
[26] J. Lukasiewicz. 1962. Blast Hypersonic Flow Analogy – Theory and Application. *American Rocket Society Journal*. 9:1341-1346.
[27] W.L.Hankey, R.D.Neumann, E.H.Flinn. 1960. Design procedures for computing aerodynamic heating at hypersonic speeds. WADC technical report.